



High-temperature steam reforming of methanol over ZnO–Al₂O₃ catalysts

Mei Yang^{a,b}, Shulian Li^a, Guangwen Chen^{a,*}

^a Dalian National Laboratory for Clean Energy, Dalian Institute of Chemical Physics, Chinese Academy of Sciences, Dalian 116023, China

^b Graduate University, Chinese Academy of Sciences, Beijing 100049, China

ARTICLE INFO

Article history:

Received 19 July 2010

Received in revised form 6 October 2010

Accepted 9 October 2010

Available online 15 October 2010

Keywords:

Methanol steam reforming

Microreactor

Hydrogen

ZnO–Al₂O₃

CO formation

ABSTRACT

In this study, a series of ZnO–Al₂O₃ catalysts with various ZnO/(ZnO + Al₂O₃) molar ratios have been evaluated for the high-temperature steam reforming of methanol, and the optimizing catalyst composition consists in the range of 0.50–0.67. The catalysts were characterized by N₂ adsorption–desorption, X-ray diffraction and UV–vis spectra. In the case of ZnO/(ZnO + Al₂O₃) > 0.5, a significant proportion of Zn could dissolve in ZnAl₂O₄, resulting in Zn-rich non-stoichiometric spinel, in which the Zn²⁺ ions located both at the tetrahedral and octahedral sites. It was noticed that such a coordination of Zn²⁺ ions in the octahedral position brought about a higher CO selectivity. Further investigation illuminated water gas shift and methanol decomposition reaction were both involved in the formation of CO. There was no noticeable deactivation for ZnO–Al₂O₃ with the ZnO/(ZnO + Al₂O₃) molar ratio of 0.50 during the 200 h continuous operation (GHSV = 17930 h⁻¹, T = 420 °C). The H₂ space time yield is 55 L h⁻¹ g_{cat}⁻¹ and the concentration of CO in the dry gaseous products was lower than 0.8%.

© 2010 Elsevier B.V. All rights reserved.

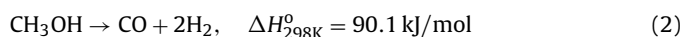
1. Introduction

PEMFCs are promising as hydrogen-based electrical power sources at a range of scales for stationary, transportation and portable power applications. Unfortunately, the commercialization of PEMFCs has been hindered by some difficulties [1], such as durability, cost and hydrogen storage and distribution, etc. Thereinto, one of the possible solutions for hydrogen storage and distribution is on board hydrogen generation from hydrocarbon fuels or renewable sources. Methanol is one of the most popular fuels due to its high H/C ratio, low boiling point and no C–C bond. Generally, there are three methods to produce hydrogen from methanol:

Steam reforming of methanol (SRM)



Decomposition of methanol (DM)



Partial oxidation of methanol (POM)



SRM has been considered as the most suitable process to obtain H₂-rich reformat for fuel cell application because of its higher hydrogen yield and low selectivity to CO which is well-known as a poison to Pt electrode of PEMFCs [2].

From a series of the open literatures dedicated to steam reforming of methanol, SRM can be classified as low and high temperature steam reforming. Low temperature steam reforming mainly focuses on Cu-based [3–15] and Pd-based [16–22] catalysts. For Cu-based catalysts, the most extensively studied catalysts are Cu/ZnO and Cu/ZnO/Al₂O₃ [7,9,10], etc. It is generally accepted that copper is the active phase. The role of Al₂O₃ is regarded to improve the surface area of the catalysts and inhibit thermal sintering of copper particles [11]. ZnO is well-known to improve the dispersion of Cu and the reducibility of CuO [5,6]. In addition, the efficiency of Cu-based catalysts can be promoted by ZrO₂, CeO₂ [4,12–14]. ZrO₂ can promote the SRM reaction and slightly reduce the concentration of CO [13]. CeO₂ can hinder the Cu sintering and enhance the thermal stability of catalysts [14]. Apart from Cu-based catalyst, Pd-based catalyst is another promising low temperature steam reforming catalyst [16–22]. Iwasa et al. [20] first found Pd/ZnO had good activity, CO₂ selectivity and thermal stability for low temperature steam reforming of methanol, and all these were attributed to the formation of PdZn alloy. Further studies [17,19] illuminated that CO₂ selectivity strongly depended on the particle size and the subsurface layers of PdZn alloy. Lately, Pd–Ga₂O₃ [21] and Pd–In₂O₃ [23] catalysts have also attracted much attention. Although Cu-based and Pd-based catalysts show good activity and selectivity to low temperature steam reforming, there are some obvious drawbacks. Cu-based catalysts are pyrophoric and easily deactivated at elevated temperature, while the high cost of Pd-based catalysts can not be neglected.

High temperature steam reforming is usually integrated with H₂ permeable membrane reactor to produce pure hydrogen. The

* Corresponding author.

E-mail address: gwchen@dicp.ac.cn (G. Chen).

use of membrane reactor offers the possibility for a compact unit in combining both the reaction and separation in a single unit. Pd-membrane reactor has been widely used for its high hydrogen selectivity and permeability [24,25]. The operating temperature of Pd-membrane reactor should be higher than 300 °C. If not, the Pd–H phase transition will occur which leads to membrane degradation. From such a point of view, SRM should be carried out above 300 °C. Jia et al. [26] prepared Ir-based catalyst which showed good activity between 380 and 480 °C with the CO selectivity above 59%. Qi et al. [27] investigated the performance of Ni–Al layered double hydroxides derived catalysts. The catalyst was durable at 390 °C, but the CO selectivity was over 10% with the methanol conversion of 35%. It can be seen that the catalysts mentioned above produced fairly high CO, which can reduce the H₂ yield and inhibit the hydrogen permeation of Pd membrane [28]. Therefore, the suppression of CO formation over the high temperature catalyst is still very essential. Matsumura and Ishibe [29] found Cu/ZnO/ZrO₂ as an active catalyst with the selectivity of CO no more than 5% at 400 °C. Although it was more durable than Cu/ZnO, Cu/ZrO₂, Cu/ZnO/Al₂O₃ at high temperature, the stability was still an issue. In our previous work, we found that ZnO–Cr₂O₃ catalyst was a promising catalyst for high temperature steam reforming [30]. ZnO was considered to be the active phase. The addition of Cr to ZnO resulted in the formation of ZnCr₂O₄ spinel and promoted the activity and stability of the catalysts. Nevertheless, Cr₂O₃ presented the significant disadvantage for its harm to environment. Of course, the high temperature steam reforming can be carried out alone besides combining with the membrane reactor. By using an efficient heat exchanger such as a microchannel heat exchanger or a microchannel reactor with microchannel heat exchanger structure, a lot of heat can be recovered through a heat exchanger between the feed and reformat gas. Meanwhile, it can be seen from the calculated results that the energy consumed in the reaction at 400 °C is only 9% higher than that at 250 °C. Most energy is consumed in the vaporization process.

To sum up, it is very attractive to develop a green, inexpensive and efficient high-temperature steam reforming catalyst with low CO concentration and long-term stability. ZnO–Al₂O₃ has been widely used as a catalyst or catalyst support for active metals [31–34]. It shows to be active for oxidative dehydrogenation of 1-butene [32] and reverse water gas shift reaction [34]. It is also a very important component of Cu/ZnO/Al₂O₃ catalyst used in methanol synthesis. In this paper, we examined the activity of ZnO–Al₂O₃ for high-temperature steam reforming of methanol. We found ZnO–Al₂O₃ exhibited high activity and generated hydrogen-rich reformat with low CO concentration, and then explored the effects of the reaction temperature, catalyst composition, gas hourly space velocity (GHSV) and steam to methanol ratio (S/M) on the activity, selectivity and stability for steam reforming of methanol.

2. Experimental

2.1. Catalyst preparation

The catalysts were prepared by a co-precipitation method at a constant pH of 7–8. The metal nitrates [Zn(NO₃)₂·6H₂O, Al(NO₃)₃·9H₂O] were dissolved into 200 ml de-ionized water. The aqueous solution of metal nitrates with a total cation concentration of 1.0M was contacted with a basic solution of aqueous ammonium with a stoichiometric molar ratio. The process was carried out by dropwise addition of both solutions into a stirred flask containing 200 ml of de-ionized water at room temperature. The precipitate formed was aged in the mother liquid for 1 h, then removed, washed with de-ionized water several times and centrifuged. The obtained deposit was dried at 90 °C for 8 h and calcined for 3 h. The catalyst was then ground, pressed, crushed and screened

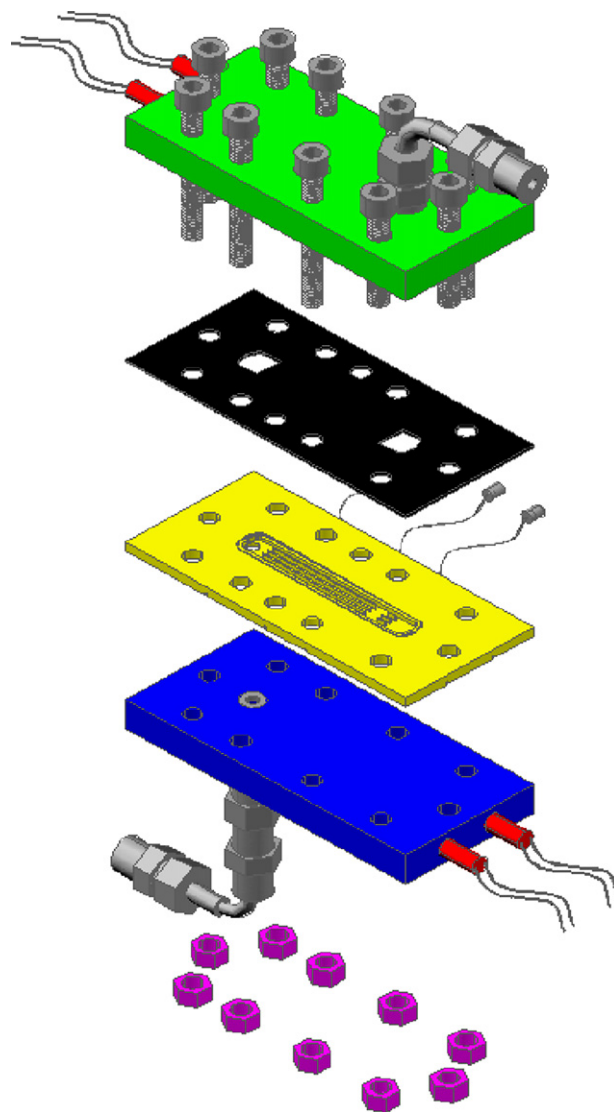


Fig. 1. Schematic diagram of the multichannel microreactor.

to 40–60 mesh (0.245–0.35 mm). The resultant ZnO–Al₂O₃ samples are designated as ZnO–X–Y, in which the symbol X represents the ZnO/(ZnO + Al₂O₃) molar ratio, while the symbol Y represents the calcination temperature. When the catalysts were calcined at 500 °C, the resultant ZnO–Al₂O₃ samples are abbreviated as ZnO–X.

2.2. Catalyst characterization

The X-ray diffraction (XRD) patterns were obtained with a PANalytical X'Pert-Pro powder X-ray diffractometer, using Cu K α monochromatized radiation ($\lambda = 0.1541$ nm) at a scan speed of 5°/min. The spectra of catalyst was collected after calcination.

The specific surface areas (S_{BET}) of the samples were measured by the BET method on an AutoChem 2910 instrument using nitrogen adsorption isotherms at 77 K (the cross section of the nitrogen molecule was taken to the 0.162 nm² [35]).

UV–vis spectra were obtained on a Cintra (GBC) apparatus with BaSO₄ as a reference.

2.3. Catalytic test

Methanol steam reforming was carried out in a multichannel microreactor (shown in Fig. 1) under atmospheric pressure. The

Table 1
BET surface areas of the catalysts with different ZnO content.

Sample	Composition (mol%)		Calcination temperature (°C)	S _{BET} (m ² /g)
	ZnO	Al ₂ O ₃		
ZnO-96	96	4	500	20
ZnO-88	88	12	500	47
ZnO-83	83	17	500	50
ZnO-75	75	25	500	55
ZnO-67	67	33	500	90
ZnO-59	59	41	500	97
ZnO-50	50	50	500	118
ZnO-24	24	76	500	229
ZnO-0	0	100	500	246

microreactor had 4 parallel channels with a width of 1.5 mm, a depth of 1.5 mm and a length of 40 mm. 0.32 g catalyst particles with the size of 40–60 mesh were packed within the channels.

A mixture of methanol and water was pumped using a HPLC pump into the vaporizer at 280 °C. The vapor was then fed into the microreactor. Subsequently, the reactor effluent passed through a condenser with a mixture of ice–water to trap the unreacted water and methanol. The flow rate of the dry reformat was measured by a soap bubble flow meter. The dry reformat were analyzed by an on-line gas chromatograph (GC 4000A, Beijing East & West Analytical Instruments Inc) equipped with a thermal conductivity detector (TCD) and a carbon molecular sieve column (TDX-01). All the data were collected when the catalytic activity was kept stable, and material balances on N₂ were calculated to verify the measurement accuracy. The flow rate of N₂ was 149 ml min⁻¹ under the conditions of 1 atm and 25 °C. When the catalysts were tested, the activity was measured at least two times. The difference in the activities measured at different times was very small. The N₂ balance was within ±3%.

In this paper, GHSV (calculated on the basis of the flow rate of methanol under the conditions of 1 atm and 25 °C), methanol conversion (X_{MeOH}), CO selectivity (S_{CO}) and H₂ space time yield (Y_{H₂}) are defined as the following:

$$\text{GHSV} = \frac{Q_{\text{MeOH}}}{V_{\text{R}}} \times 60 \quad (4)$$

$$X_{\text{MeOH}} = \frac{n_{\text{CO}} + n_{\text{CO}_2} + n_{\text{CH}_4}}{n_{\text{M},0}} \times 100 \quad (5)$$

$$S_{\text{CO}} = \frac{n_{\text{CO}}}{n_{\text{CO}} + n_{\text{CO}_2} + n_{\text{CH}_4}} \times 100 \quad (6)$$

$$Y_{\text{H}_2} = \frac{n_{\text{H}_2}}{m_{\text{cat}}} \times 22.4 \times 60 \quad (7)$$

where Q_{MeOH} is the gas flow rate of methanol, ml min⁻¹; V_R is the micro reactor volume, ml; n_{CO}, n_{CO₂}, n_{CH₄} and n_{H₂} is the molar flow rate of CO, CO₂, CH₄ and H₂ in the dry reformat, mol/min; n_{M,0} is the molar flow rate of methanol in the mixture feed, mol/min; m_{cat} is the weight of the catalyst, g.

3. Results and discussion

3.1. Catalyst characterization

3.1.1. BET surface area

The relation of catalyst composition and BET surface area is summarized in Table 1. The surface area increases significantly with the incorporation of Al₂O₃. For example, the surface area of ZnO-96 is 20 m²/g. When the amount of Al₂O₃ increases to 50%, the surface area increases to 118 m²/g. ZnO-0 maintains the largest surface area of 228 m²/g.

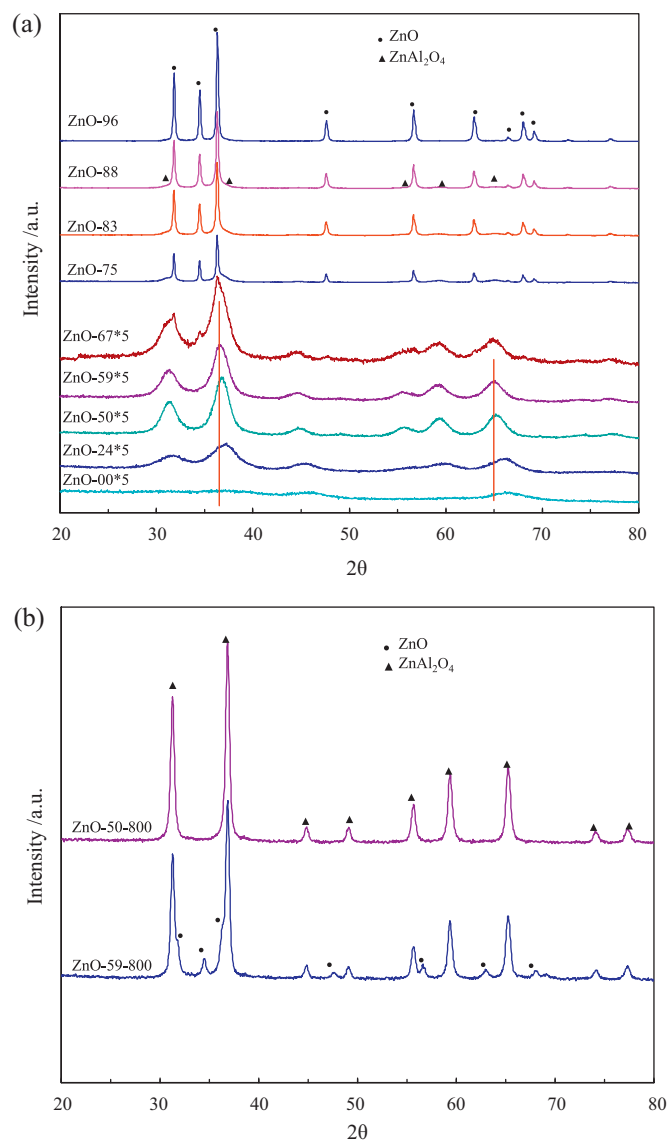


Fig. 2. The XRD patterns of the catalysts (a) with different ZnO content and (b) ZnO-50-800 and ZnO-59-800.

3.1.2. X-ray diffraction (XRD)

Fig. 2a shows the XRD patterns of ZnO–Al₂O₃ samples obtained by calcination of the precursors at 500 °C. In agreement with the data provided by the International Center for Diffraction Data (ICDD), all reflections can be assigned to zincite, zinc aluminum spinel or gamma-alumina. Only zincite is identified for ZnO-96 in Fig. 2a. This is not surprising because the concentration and crystalline of ZnAl₂O₄ in ZnO-96 may be below the detection limit of XRD instrument. In the case of ZnO-67, ZnO-75, ZnO-83 and ZnO-88, the samples contain two phases, zincite and zinc aluminum spinel. The intensities of the XRD peaks corresponding to zincite become lower with the decrease of ZnO, whereas those of ZnAl₂O₄ become more obvious. For ZnO-59, ZnO-50 and ZnO-24, only zinc aluminum spinel is observed. Furthermore, the characteristic peaks of zinc aluminum spinel are found to shift to the larger angle side with the decreasing ZnO. For ZnO-0, three broad peaks at 2θ = 36.8°, 45.7° and 66.4° in the XRD curve indicate the presence of poorly crystalline γ-Al₂O₃ in accordance with the literatures [36,37].

The XRD patterns of ZnO-50-800 and ZnO-59-800 samples obtained by calcination of the precursors at 800 °C are compared in Fig. 2b. It can be seen that the zinc aluminum spinel peaks become

Table 2
Comparison the lattice parameters of the catalysts with different ZnO contents*.

Sample	Phases	<i>a</i> (nm)
ZnO-59	Spinel	0.8130(5)
ZnO-59-800	Zincite	
	Spinel	0.8092(8)
ZnO-50	Spinel	0.8100(4)
ZnO-50-800	Spinel	0.8092(5)
ZnO-24	Spinel	0.8036(4)

* The lattice parameters of ZnAl₂O₄ in ZnO-96, ZnO-88, ZnO-83 and ZnO-75 could not be calculated because ZnAl₂O₄ peaks in these samples were very weak. The lattice parameter of ZnAl₂O₄ in ZnO-67 was also not shown in this table due to its significant overlapping with ZnO.

stronger, and no other impurity phase is found for ZnO-50-800. In contrast, the XRD peaks corresponding to zincite are clearly discerned together with the more intense peaks of zinc aluminum spinel for ZnO-59-800.

II–III spinel (AB₂O₄) is an important material for its high thermal and mechanical stability. Normal spinel has 8 bivalent ions in tetrahedral sites and 16 trivalent ions in octahedral sites, while inverse spinel has 8 trivalent ions in tetrahedral sites and 8 bivalent ions together with 8 trivalent ions in octahedral sites. Compared with the stoichiometric spinel, non-stoichiometric spinel is also very common. B₂O₃ oxide can dissolve into AB₂O₄ to form B-rich non-stoichiometric spinel, AO·*n*B₂O₃ (*n* > 1) [38]. Tetrahedral A²⁺ ions can be substituted by B³⁺ ions accompanied by the formation of cation vacancies. In general, AO is hardly dissolved in spinel lattice above its stoichiometric composition. However, some studies suggest that a significant proportion of Zn can enter the ZnM₂O₄ structure (M = Fe, Cr) at the octahedral sites, resulting in a Zn-rich non-stoichiometric spinel [39,40]. Consequently, more oxygen vacancies are formed. In our study, we find a significant proportion of Zn can also enter ZnAl₂O₄ to form Zn-rich non-stoichiometric spinel.

It can be seen from Fig. 2a that ZnO and Al₂O₃ can be easily transformed into ZnAl₂O₄ once heated at 500 °C. Many studies have suggested that ZnAl₂O₄ has a close-packed face centered cubic structure of normal spinel phase [41]. For ZnO-50 with the Zn/Al mole ratio of 0.5, the XRD pattern displays no impurity phase besides ZnAl₂O₄ even when the precursor is calcined at 800 °C shown in Fig. 2b. This indicates that the structure of ZnO-50 is stoichiometric ZnAl₂O₄ of high purity. Therefore, Zn²⁺ ions incorporate exclusively at the tetrahedral sites in ZnO-50. For ZnO-59 (Zn/Al ≈ 0.72), 18% ZnO (calculated value) is expected to be detected with respect to the ZnAl₂O₄ stoichiometry. However, there is only ZnAl₂O₄ spinel as the detectable phase. When the precursor is calcined at 800 °C, crystalline ZnO appears as a secondary phase (Fig. 2b). The excessive Zn in ZnO-59 is assumed to be inside ZnAl₂O₄ to form non-stoichiometric spinel, accompanied by the formation of oxygen vacancies.

The lattice parameters of ZnAl₂O₄ in the samples with different zinc content are summarized in Table 2. It can be seen that the lattice parameter is related to the sample's composition. Lattice parameter of ZnO-50 (stoichiometric ZnAl₂O₄) is 0.8100 nm, a little higher than the reported value of ZnAl₂O₄ (*a* = 0.80848 nm, JCPDS File 5-669). This lattice parameter expansion is possibly due to an effective negative pressure which is created by the competition between the long-range Coulomb attractive and the short-range repulsive interaction in ionic nanocrystals [42]. As discussed above, the structure of ZnO-59 is Zn-rich non-stoichiometric spinel. If it is true, then the lattice parameter of ZnO-59 will be larger than that of ZnO-50. This is because the size of Al³⁺ ions (ionic radius (IR) in coordination 4 (CN4) IR(CN4) = 0.039 nm, IR(CN6) = 0.0535 nm) is smaller than that of Zn²⁺ ions (IR(CN4) = 0.060 nm, IR(CN6) = 0.074 nm) [43]. As shown

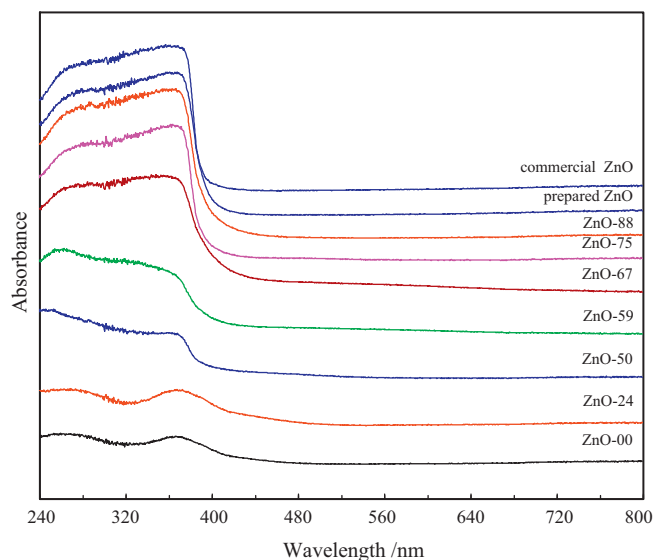


Fig. 3. The UV–vis absorption spectra of the catalysts with different ZnO content.

in Table 2, it is indeed the case. This change in the lattice parameter validates the hypothesis that excessive Zn enters ZnAl₂O₄ to form Zn-rich non-stoichiometric spinel. Consequently, the Zn²⁺ ions are present at both tetrahedral and octahedral sites. It is an unusual co-ordination for Zn²⁺ ions which have tetrahedral co-ordination in ZnO and stoichiometric ZnAl₂O₄. Lattice parameter of ZnO-24 is smaller than that of ZnO-50 because of the formation of Al-rich spinel phase, in which Al³⁺ ions are present at both tetrahedral and octahedral sites, in accordance with the results of Wang et al. [44]. On the other hand, the lattice parameter of ZnO-59-800 is smaller than that of ZnO-59 but equal to that of ZnO-50-800. This result demonstrates that high calcination temperature can transform non-stoichiometric phase into stoichiometric phase associated by the appearance of crystalline ZnO.

3.1.3. UV–vis characterization

UV–vis absorption experiments provide further insight into the samples. The UV–vis absorption spectra of the samples with different ZnO content are compared with commercial and self-prepared ZnO spectra in Fig. 3. There is intense absorption below the wavelength of 400 nm for commercial and self-prepared ZnO, which is known as a strong absorption of ZnO. This absorption is corresponded to a charge-transfer process from the valence band (O 2p orbitals) to the conduction band (Zn 4s orbitals) [45,46]. The absorption spectra of ZnO-96, ZnO-88, ZnO-75 and ZnO-67 show the characteristic absorption of ZnO. This result evidences the presence of ZnO in these samples which is in agreement with XRD results. The absorption spectra of ZnO-50 (stoichiometric ZnAl₂O₄) is in accordance with the absorption spectra of ZnAl₂O₄ in the literature [47]. There are two absorption peaks. The first one below 400 nm is in the similar wavelength region but significantly weaker than that of ZnO. The second one with the peak wavelength of 260 nm is a little stronger than the first one, which is due to electronic excitations between filled O 2p orbitals and empty Al 3s orbitals, with possibly some Al 3p wave function mixing. The absorption spectra of ZnO-59 is similar with that of ZnO-50, but different from those of ZnO-96, ZnO-88, ZnO-83, ZnO-75 and ZnO-67. This result further proves the hypothesis that excessive Zn can enter ZnAl₂O₄ to form Zn-rich non-stoichiometric spinel. The absorption spectra of ZnO-24 is similar with that of ZnO-0, which has two absorption within the wavelength of 240–320 nm and 320–420 nm, respectively. It indicates that excessive amorphous Al₂O₃ is present in ZnO-24, which could not be detected by XRD.

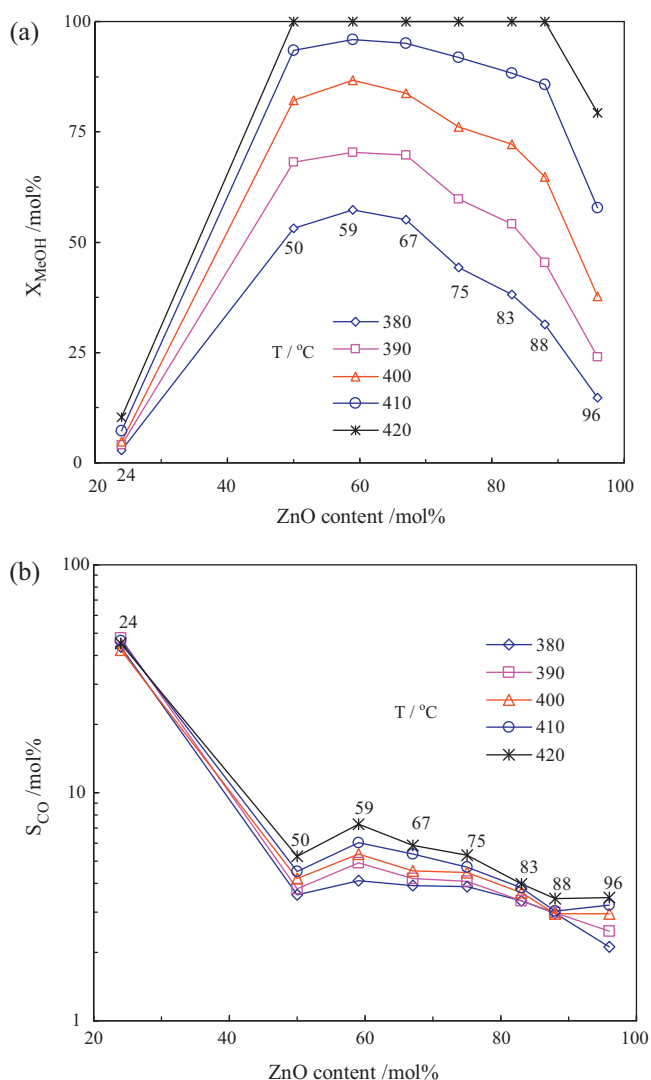


Fig. 4. (a) Methanol conversion and (b) CO selectivity as a function of zinc content. GHSV = 11,800 h⁻¹, S/M = 1.4.

3.2. Catalytic activity for SRM

In this set of experiments, we explored the effects of the reaction temperature, catalyst composition, GHSV and the molar ratio of steam to methanol (S/M) on the activity, selectivity and stability of catalysts for steam reforming of methanol.

3.2.1. Effect of reaction temperature

Fig. 4a illustrates the methanol conversion as a function of the zinc content over the temperature range of 380–420 °C. The experiments were carried out under the reaction conditions of S/M = 1.4 and GHSV = 11,800 h⁻¹. Pure Al₂O₃ nearly has no activity for steam reforming of methanol (not shown in the Fig. 4a). Hence, the active sites for SRM can possibly be associated with Zn²⁺ ions, which is consistent with the work of Cao et al. [48] and Hong and Ren [49]. It is evident from Fig. 4a that the methanol conversion increases with the reaction temperature over all of the catalysts. At 420 °C, the methanol conversion reaches to 100% for all samples except ZnO-96 and ZnO-24. Furthermore, the activity of catalyst increases continuously with increasing Al₂O₃ content, and the samples with the charged ratio, ZnO/(ZnO + Al₂O₃) molar ratio of 0.50–0.67, exhibit the highest activity. When the ZnO/(ZnO + Al₂O₃) ratio is further decreased, the catalyst activity decreases. Low methanol

conversion is observed over ZnO-24 sample. The density of Zn²⁺ ions decreases with the increasing Al₂O₃ content, which would result in a loss in activity of catalyst. However, in the case of ZnO/(ZnO + Al₂O₃) > 0.67, the activity increases with the increasing Al₂O₃ content. This enhancement in activity may be partly due to the increase of the surface area of catalysts (Table 1). For ZnO-59 and ZnO-50, the catalytic activity is similar. With respect to the results of XRD and UV–vis spectra, in ZnO-59 (Zn-rich non-stoichiometric spinel), Zn²⁺ ions occupy both the tetrahedral and octahedral sites, whereas Zn²⁺ ions only locate at the tetrahedral sites in ZnO-50 (stoichiometric spinel). In earlier studies, it was suggested that the catalytic activity of a metal ions generally higher when it is present on octahedral sites than when it is present on tetrahedral sites [50]. However, such a coordination of Zn²⁺ ions in the octahedral sites does not show great effect on the catalytic activity for SRM in our study, whereas causes a higher CO selectivity as shown in Fig. 4b. The methanol conversion over ZnO-24 is only 10.4% even at 420 °C. The poor activity may be partly due to the lower Zn²⁺ ions concentration in the sample. On the other hand, the excessive amorphous Al₂O₃ in the sample may also hinder the reforming reaction [51].

All samples except ZnO-24 perform well in SRM. Hence, we can conclude that Zn²⁺ ions in both in ZnO and Zn_{1+x}Al_{2-2/3x}O₄ (x ≥ 0, Zn-rich non-stoichiometric or stoichiometric spinel) can be the active sites for SRM.

The CO selectivity is shown in Fig. 4b as a function of the zinc content. It can be seen that the CO selectivity of ZnO-24 is fairly higher, which might be caused by the excessive amorphous Al₂O₃ in the sample. It has been reported that methanol can be decomposed to H₂ + CO over Al₂O₃ [52]. As can be seen from Fig. 4a and b, the CO selectivity follows the order: ZnO-59 > ZnO-50, whereas these catalysts exhibit similar methanol conversion. As mentioned above, Zn²⁺ ions occupy both the tetrahedral and octahedral sites in ZnO-59, whereas Zn²⁺ ions only locate at the tetrahedral sites in ZnO-50. The trend of total number of octahedral Zn²⁺ ions is ZnO-59 > ZnO-50. A correlation between CO selectivity and total number of octahedral Zn²⁺ ions can be expected. Therefore, the octahedral Zn²⁺ ions may contribute to the higher CO selectivity. This indicates that the Zn²⁺ ions in octahedral sites are not as selective as those in tetrahedral sites to CO₂ + H₂ in SRM. ZnO-67, ZnO-75, ZnO-83, ZnO-88 and ZnO-96 consist of a mixture of ZnO and Zn-rich non-stoichiometric spinel. It is difficult to identify the individual contribution of ZnO and Zn-rich non-stoichiometric spinel to CO selectivity based on the results obtained so far. However, it is clear that the amount of Zn-rich non-stoichiometric spinel increases with the decreasing ZnO content (Fig. 2a). In other words, the amount of octahedral Zn²⁺ ions rises with the decreasing ZnO content. This may to some extent be related to the trend of CO selectivity as follows: ZnO-67 > ZnO-75 > ZnO-83 > ZnO-88 > ZnO-96. Additionally, a higher temperature favors a higher CO selectivity over the temperature range investigated. This increase of CO is possibly due to the reverse water gas shift reaction, which is preferential at higher temperature owing to the thermodynamic equilibrium.

3.2.2. Effect of gas hourly space velocity

The conversion of methanol and the selectivity of CO over all catalysts are plotted in Fig. 5a and b as a function of GHSV. The experiments were carried out under the reaction conditions of S/M = 1.4 and reaction temperature = 410 °C. The GHSV varied from 11,800 h⁻¹ to 35,400 h⁻¹. As shown in Fig. 5a, the methanol conversion decreases as GHSV increases. Increasing GHSV decreases the contact time. A decrease in the contact time, of course, results in a lower conversion. As shown in Fig. 5b, it is evident that the CO selectivity declines gradually with increasing GHSV.

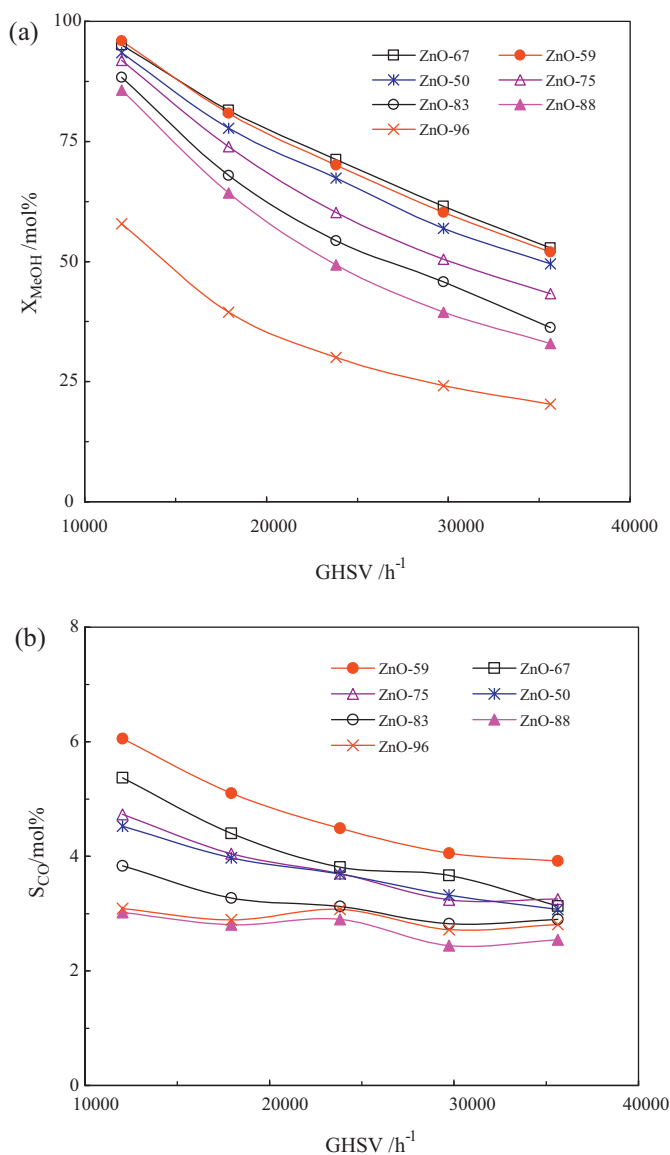


Fig. 5. (a) Methanol conversion and (b) CO selectivity as a function of GHSV. Reaction temperature = 410 °C, S/M = 1.4.

Furthermore, the route of CO formation over ZnO–Al₂O₃ catalysts was investigated. Initially, a methanol decomposition/WGS reaction sequential route has been speculated in the steam reforming process [53]. However, this explanation becomes unacceptable since many results have shown that the CO level in the reformat gas is dramatically lower than the predicted value from WGS equilibrium [54]. This conclusion is reconfirmed in our study. As shown in Fig. 6, the CO concentration in the steam reforming process is far below than the value obtained from WGS equilibrium, indicating WGS reaction is not involved in the reaction pathway of steam reforming of methanol. According to literatures [12,55], there are two CO formation mechanisms: RWGS and DM. In the first mechanism, CO selectivity decreases with the decreasing contact time, whereas in the later one CO selectivity is independent of the contact time. In order to clarify the route responsible for CO formation, the effect of contact time (W/F , $g \text{ min cm}^{-3}$) on the CO selectivity was investigated over ZnO-59 and ZnO-50 by varying the GHSV. Fig. 7 presents a plot of CO selectivity versus the contact time (W/F). The CO selectivity first declines gradually with the decrease of contact time and then reaches to a constant level at the value of the contact time lower than $3.9 \times 10^{-4} g \text{ min cm}^{-3}$. This indicates that

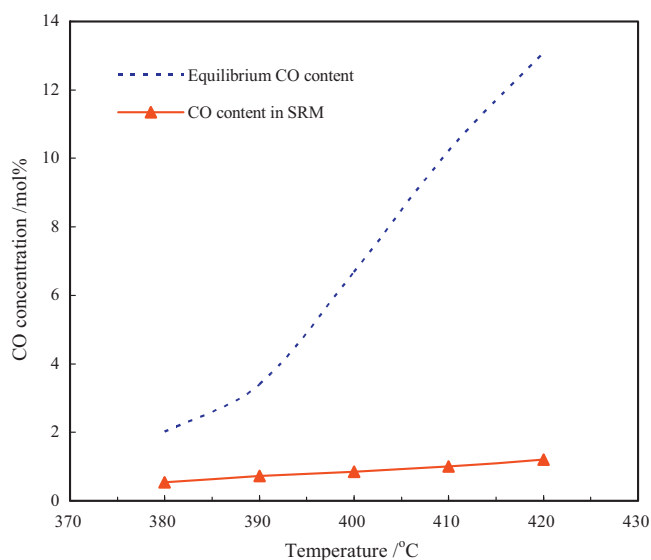


Fig. 6. Comparison of the CO concentration between SRM over ZnO-59 and WGS equilibrium.

both reactions, DM and RWGS are involved in the formation of CO. As mentioned previously, the octahedral Zn²⁺ ions in Zn-rich non-stoichiometric spinel give rise to a higher CO selectivity. Nevertheless, it is not yet clear which reaction, DM or RWGS, is more favorable over the octahedral Zn²⁺ ions. Further investigation is currently under way to make this question clear.

Water gas shift reaction (WGS)



Reverse water gas shift reaction (RWGS)



3.2.3. Effect of steam to methanol ratio

The effect of steam to methanol (S/M) ratio on the methanol conversion and CO selectivity on ZnO-59 catalyst was studied by varying the amount of water into the reactor while keeping a constant amount of methanol. Fig. 8 shows the methanol conversion

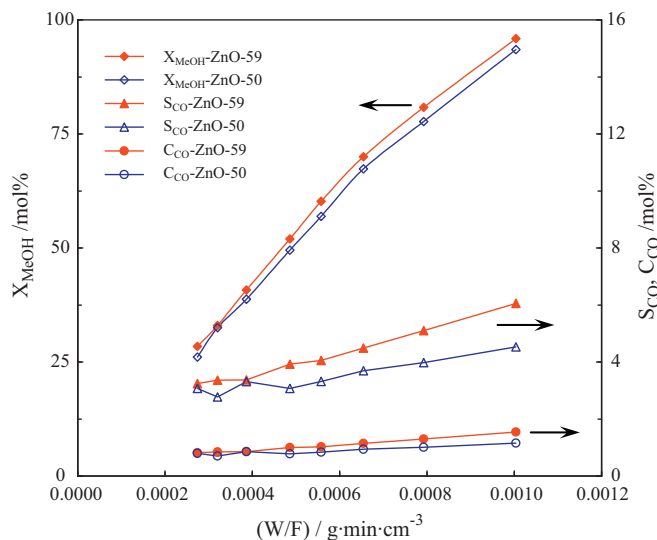


Fig. 7. Methanol conversion, CO selectivity and CO concentration (C_{CO}) as a function of the contact time (W/F) over ZnO-59 and ZnO-50. Reaction temperature = 410 °C, S/M = 1.4.

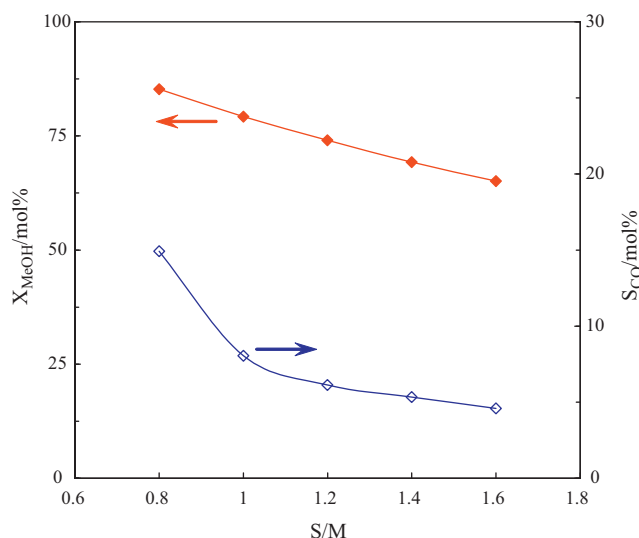


Fig. 8. Methanol conversion and CO selectivity as a function of S/M for ZnO-59. Reaction temperature = 420 °C, GHSV = 28,690 h⁻¹.

and CO selectivity as a function of S/M ratio under the reaction conditions of GHSV = 28,690 h⁻¹ and reaction temperature = 420 °C. Some researchers suggested that water and methanol compete for the same adsorption sites on ZnO [56]. Methanol is easily adsorbed onto the surface of ZnO to form methoxy species, which decompose into CO and H₂ eventually in the absence of water. When water is added into the feed, methoxy species are easily oxidized into formate species, which decompose into CO₂ and H₂ ultimately. The rising concentration of water reduces the amount of absorptive methanol, therefore, the methanol conversion decreases monotonically with the increase in S/M, with a similar drop in the CO selectivity (as shown in Fig. 8). At S/M ratio = 0.8, the excessive methanol decomposes to H₂ and CO leading to a higher CO selectivity. As S/M ratio rises from 0.8 to 1.0, the CO selectivity declines from 15% to 8% dramatically. This result indicates that the decomposition of excessive methanol is suppressed by the increasing steam partial pressure. In addition, as stated above, the CO is partly produced by RWGS. Hence, another possibility for this decreasing CO selectivity is that the equilibrium of RWGS moves to the right to generate less CO as S/M ratio increases. It is also the reason why the CO selectivity still keeps going down as S/M ratio further increases from 1.0

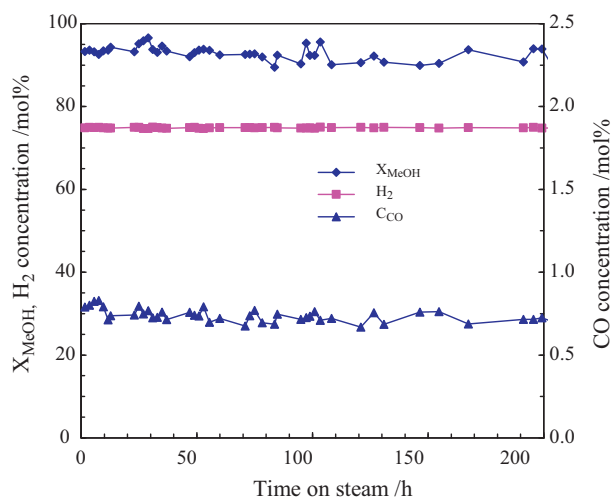


Fig. 9. Stability test over ZnO-50 catalyst. Reaction temperature = 420 °C, S/M = 1.4, GHSV = 17,930 h⁻¹.

to 1.6. The result suggests that a higher concentration of water is beneficial for reduction of CO.

3.2.4. Catalyst stability

The stability of ZnO-50 catalyst was evaluated by running for 200 h under the reaction condition of reaction temperature = 420 °C, S/M = 1.4 and GHSV = 17,930 h⁻¹. As shown in Fig. 9, ZnO-50 exhibits a high activity and stability. The methanol conversion above 90% is attained in the 200 h test. The CO concentration remains to be lower than 0.8%, and the H₂ concentration is nearly constant. The spinel structure is well known for its thermal stability. Cao et al. [30] reported that the formation of ZnCr₂O₄ spinel structure can enhance the stability of Zn–Cr catalyst. Park et al. [34] found ZnAl₂O₄ is very stable for RWGS. In our work, ZnAl₂O₄ also shows good stability, which can be used as a promising efficient catalyst in high-temperature steam reforming of methanol.

4. Conclusion

In summary, ZnO–Al₂O₃ catalysts prepared by a co-precipitation method have been found to exhibit good catalytic activity for high temperature steam reforming of methanol. The catalytic performances were markedly affected by the composition of catalysts. The best performance was obtained over the catalysts with the ZnO/(ZnO + Al₂O₃) ratio of 0.5–0.67. In this range, the methanol conversion was similar but the CO selectivity was different. The CO selectivity of ZnO-59 was higher than that of ZnO-50. Subsequently, such a difference in CO selectivity was correlated with XRD and UV–vis spectra results and the octahedral Zn²⁺ ions in Zn-rich non-stoichiometric ZnAl₂O₄ were proposed to be responsible for such a higher CO selectivity.

Then the route of CO formation was investigated. The CO concentration obtained from WGS equilibrium was much higher than that in the steam reforming of methanol over ZnO-59, implying WGS was not involved in the pathway of the steam reforming of methanol. Furthermore, we found RWGS and DM were both involved in the formation of CO.

At last, a life test was carried out to check the stability of ZnO-50 at a GHSV as high as 17,930 h⁻¹. During the 200 h continuous operation, no noticeable deactivation was found. The H₂ concentration remained constant and the CO concentration was always lower than 0.8%. The excellent thermal stability and good activity of catalyst demonstrated ZnO–Al₂O₃ a promising catalyst for high temperature steam reforming of methanol.

Acknowledgments

The work reported in this article was financially supported by research grants from the National Natural Science Foundation of China (No. 20906087), Ministry of Science and Technology of China (No 2006AA020101). Thanks to Ph.D. Yong Men and Yuchao Zhao for their instructive discussion about this work.

References

- [1] F.A. de Bruijn, V.A.T. Dam, G.J.M. Janssen, Fuel Cells 8 (2008) 3–22.
- [2] Q.F. Li, R.H. He, J.O. Jensen, N.J. Bjerrum, Chemistry of Materials 15 (2003) 4896–4915.
- [3] T. Fukunaga, N. Ryumon, N. Ichikuni, S. Shimazu, Catalysis Communications 10 (2009) 1800–1803.
- [4] S.D. Jones, H.E. Hagelin-Weaver, Applied Catalysis B-Environmental 90 (2009) 195–204.
- [5] S.D. Jones, L.M. Neal, H.E. Hagelin-Weaver, Applied Catalysis B-Environmental 84 (2008) 631–642.
- [6] P. Kurr, I. Kasatkin, F. Girgsdies, A. Trunschke, R. Schlogl, T. Ressler, Applied Catalysis A-General 348 (2008) 153–164.
- [7] A. Mastalir, A. Patzko, B. Frank, R. Schomacker, T. Ressler, R. Schlogl, Catalysis Communications 8 (2007) 1684–1690.

- [8] Y. Matsumura, H. Ishibe, *Applied Catalysis B-Environmental* 86 (2009) 114–120.
- [9] T. Shishido, Y. Yamamoto, H. Morioka, K. Takehira, *Journal of Molecular Catalysis A-Chemical* 268 (2007) 185–194.
- [10] L.C. Wang, Y.M. Liu, M. Chen, Y. Cao, H.Y. He, G.S. Wu, W.L. Dai, K.N. Fan, *Journal of Catalysis* 246 (2007) 193–204.
- [11] L. Alejo, R. Lago, M.A. Pena, J.L.G. Fierro, *Applied Catalysis A-General* 162 (1997) 281–297.
- [12] J.P. Breen, J.R.H. Ross, *Catalysis Today* 51 (1999) 521–533.
- [13] G. Huang, B.J. Liaw, C.J. Jhang, Y.Z. Chen, *Applied Catalysis A-General* 358 (2009) 7–12.
- [14] Y.Y. Liu, T. Hayakawa, K. Suzuki, S. Hamakawa, *Applied Catalysis A-General* 223 (2002) 137–145.
- [15] Y. Matsumura, H. Ishibe, *Journal of Catalysis* 268 (2009) 282–289.
- [16] T. Conant, A.M. Karim, V. Lebarbier, Y. Wang, F. Girgsdies, R. Schlogl, A. Datye, *Journal of Catalysis* 257 (2008) 64–70.
- [17] A. Karim, T. Conant, A. Datye, *Journal of Catalysis* 243 (2006) 420–427.
- [18] A.M. Karim, T. Conant, A.K. Datye, *Physical Chemistry Chemical Physics* 10 (2008) 5584–5590.
- [19] C. Rameshan, W. Stadlmayr, C. Weilach, S. Penner, H. Lorenz, M. Havecker, R. Blume, T. Rocha, D. Teschner, A. Knop-Gericke, R. Schlogl, N. Memmel, D. Zemlyanov, G. Rupprechter, B. Klotzer, *Angewandte Chemie-International Edition* 49 (2010) 3224–3227.
- [20] N. Iwasa, S. Kudo, H. Takahashi, S. Masuda, N. Takezawa, *Catalysis Letters* 19 (1993) 211–216.
- [21] S. Penner, H. Lorenz, W. Jochum, M. Stoger-Pollach, D. Wang, C. Rameshan, B. Klotzer, *Applied Catalysis A-General* 358 (2009) 193–202.
- [22] H. Lorenz, S. Turner, O.I. Lebedev, G. Van Tendeloo, B. Klotzer, C. Rameshan, K. Pfaller, S. Penner, *Applied Catalysis A-General* 374 (2010) 180–188.
- [23] Y. Men, G. Kolb, R. Zapf, M. O'Connell, A. Ziogas, *Applied Catalysis A-General* 380 (2010) 15–20.
- [24] S. Hara, K. Sakaki, N. Itoh, *Industrial and Engineering Chemistry Research* 38 (1999) 4913–4918.
- [25] R. Dittmeyer, V. Hollein, K. Daub, *Journal of Molecular Catalysis A-Chemical* 173 (2001) 135–184.
- [26] J.S. Jia, J. Zhou, C.X. Zhang, Z.S. Yuan, S.J. Wang, L. Cao, S.D. Wang, *Applied Catalysis A-General* 341 (2008) 1–7.
- [27] C.X. Qi, J.C. Amphlett, B.A. Peppley, *Catalysis Communications* 11 (2009) 71–76.
- [28] S. Hara, W.C. Xu, K. Sakaki, N. Itoh, *Industrial and Engineering Chemistry Research* 38 (1999) 488–492.
- [29] Y. Matsumura, H. Ishibe, *Applied Catalysis B-Environmental* 91 (2009) 524–532.
- [30] W.Q. Cao, G.W. Chen, J.C. Chu, S.L. Li, Q. Yuan, *Chinese Journal of Catalysis* 27 (2006) 895–898.
- [31] M. Lenarda, L. Storaro, R. Frattini, M. Casagrande, M. Marchiori, G. Capannelli, C. Uliana, F. Ferrari, R. Ganzerla, *Catalysis Communications* 8 (2007) 467–470.
- [32] J.A. Toledo, P. Bosch, M.A. Valenzuela, A. Montoya, N. Nava, *Journal of Molecular Catalysis A-Chemical* 125 (1997) 53–62.
- [33] M. Nilsson, K. Jansson, P. Jozsa, L.J. Pettersson, *Applied Catalysis B-Environmental* 86 (2009) 18–26.
- [34] S.W. Park, O.S. Joo, K.D. Jung, H. Kim, S.H. Han, *Applied Catalysis A-General* 211 (2001) 81–90.
- [35] H.L. Castricum, A. Sah, R. Kreiter, D.H.A. Blank, J.F. Vente, J.E. ten Elshof, *Journal of Materials Chemistry* 18 (2008) 2150–2158.
- [36] S.J. Miao, R.N. d'Alnoncourt, T. Reinecke, I. Kasatkin, M. Behrens, R. Schlogl, M. Muhler, *European Journal of Inorganic Chemistry* (2009) 910–921.
- [37] J. Zhang, H.Y. Xu, X.L. Jin, Q.J. Ge, W.Z. Li, *Applied Catalysis A-General* 290 (2005) 87–96.
- [38] W.T. Donlon, T.E. Mitchell, A.H. Heuer, *Journal of Materials Science* 17 (1982) 1389–1397.
- [39] D. Makovec, M. Drogenik, *Journal of Nanoparticle Research* 10 (2008) 131–141.
- [40] G. Delpiero, F. Trifiro, A. Vaccari, *Journal of the Chemical Society-Chemical Communications* (1984) 656–658.
- [41] N.J. van der Laag, M.D. Snel, P.C.M.M. Magusin, G. de With, *Journal of the European Ceramic Society* 24 (2004) 2417–2424.
- [42] V. Perebeinos, S.W. Chan, F. Zhang, *Solid State Communications* 123 (2002) 295–297.
- [43] R.D. Shannon, *Acta Crystallographica Section A* 32 (1976) 751–767.
- [44] F. Wang, H.B. Huang, S.G. Yang, *Journal of the European Ceramic Society* 29 (2009) 1387–1391.
- [45] A. Hernandez, L. Maya, E. Sanchez-Mora, E.M. Sanchez, *Journal of Sol-Gel Science and Technology* 42 (2007) 71–78.
- [46] S. Sakthivel, S.U. Geissen, D.W. Bahnemann, V. Murugesan, A. Vogel, *Journal of Photochemistry and Photobiology A-Chemistry* 148 (2002) 283–293.
- [47] S.K. Sampath, J.F. Cordaro, *Journal of the American Ceramic Society* 81 (1998) 649–654.
- [48] W.Q. Cao, G.W. Chen, S.L. Li, Q. Yuan, *Chemical Engineering Journal* 119 (2006) 93–98.
- [49] X.L. Hong, S.Z. Ren, *International Journal of Hydrogen Energy* 33 (2008) 700–708.
- [50] G.K. Boreskov, *Academic press* 15 (1964) 286.
- [51] P.H. Matter, D.J. Braden, U.S. Ozkan, *Journal of Catalysis* 223 (2004) 340–351.
- [52] J.C. Brown, E. Gulari, *Catalysis Communications* 5 (2004) 431–436.
- [53] E. Santacesaria, S. Carra, *Applied Catalysis* 5 (1983) 345–358.
- [54] J.P. Breen, F.C. Meunier, J.R.H. Ross, *Chemical Communications* (1999) 2247–2248.
- [55] H. Purnama, T. Ressler, R.E. Jentoft, H. Soerijanto, R. Schlogl, R. Schomacker, *Applied Catalysis A-General* 259 (2004) 83–94.
- [56] D. Chadwick, K.G. Zheng, *Catalysis Letters* 20 (1993) 231–242.